Single-γ decays of $\eta'(958)$, $\omega(783)$, $\phi(1019)$, and $\Xi^{*-}(1535)$ †

G. R. Kalbfleisch and R. C. Strand
Brookhaven National Laboratory, Upton, New York 11973

J. W. Chapman
University of Michigan, Ann Arbor, Michigan 48104

(Received 30 October 1974)

We present direct evidence on single-γ decays in which the γ rays were converted to electron showers in tantalum plates or leaded-glass windows installed in the BNL 31-in. bubble chamber or in its 2 at.% neon-hydrogen filling. A > 90%-pure sample of 135 $\eta' \to \pi^+\pi^-\gamma$ events is obtained. The Dalitz-plot projections show the ρ meson and the sine-squared angular dependence clearly. The asymmetry between π^+ and π^- mesons in the decay is found to be 0 ± 0.1. In addition, upper limits to the following decay modes are found: $(\eta' \to \omega\gamma) \leq 0.05$, $(\omega \to \pi^+\pi^-\gamma) \leq 0.06$, $(\phi \to \pi^+\pi^-\gamma) \leq 0.06$, and $(\Xi^{*-}(1535) \to \Xi^-\gamma) \leq 0.04$, all at the 90% confidence level.

I. INTRODUCTION

We report a study of single-photon decays of $\eta'(958)$, $\omega(783)$, $\phi(1019)$, and $\Xi^{*-}(1535)$ in which the γ ray is detected by conversion. This study is based on 1.1 million pictures (approximately 40 events per microbarn) of the hydrogen-filled 31-in. BNL bubble chamber, with an admixture of 4 mole-percent neon. The chamber was fitted with 2 (or 3) tantalum plates and two leaded-glass windows of about 1 radiation-length thickness each. The chamber was exposed to a 2.18-GeV/c K^- beam at the Brookhaven AGS in three runs.[1]

Previous studies of the $\eta' \to \rho^0\gamma$ decay mode have been made using indirect kinematic identification, which leaves a substantial background due to neutral-pion production. The purer samples obtained here with γ detection give much greater confidence in all results relating to these radiative decays, especially the (lack of) asymmetry in $\eta' \to \rho\gamma$ decay.

II. PLATE ARRAY

A large fraction of the solid angle seen by events produced in the 31-in. BNL bubble chamber was subtended by an array of tantalum and leaded-glass plates, shown schematically in Fig. 1. A small hydrogen volume behind the plates opposite the event volume allows the electron-positron tracks from conversion showers to be observed. The three cameras of the chamber view the event volume through the front leaded-glass window. The light from the arc flash is retrodirected by the Scotchlite on the "racetrack" and on the rear panel behind the rear leaded glass. The leaded-glass windows were fabricated from SF1 glass purchased from Ohara Glass, Japan. The windows were polished optically flat and coated with anti-reflective coatings by Tinsley Laboratories, Berkeley, California, and Optical Coating Laboratories, Santa Rosa, California, respectively. Opposite the expansion part, a side plate of tantalum was installed in the bottom of the chamber. At the downstream end other tantalum plates were installed. In the first run (first 0.5 million pictures, rolls 700 through 960) only the larger endplate was installed at the position shown "dotted" in Fig. 1. In the second and third runs (rolls 1 through 550) increased coverage of the downstream solid angle was provided by moving the larger endplate about 4 cm upstream and adding a smaller second plate below the "racetrack" as shown in Fig. 1. The leaded-glass windows are 2.6 cm thick and the tantalum plates 0.6 cm thick, i.e., about 1 radiation-length thick each. The over-all detection efficiency of the array for γ's is about 35%. The specifications, fabrication, and installation (and removal) of the plate array for each of the three runs was carried out by John Koehler.

Three of the $\eta' \to \rho\gamma$ events detected (see below) are shown in Figs. 2, 3, and 4. Figure 2 shows an event in which the γ converts in the liquid to an electron-positron pair. Figure 3 shows an event in which the γ showers in the rear leaded-glass window and Fig. 4 shows one in the side tantalum plate.

III. SELECTION OF EVENTS

The reactions of interest in this paper are (MM stands for missing mass)

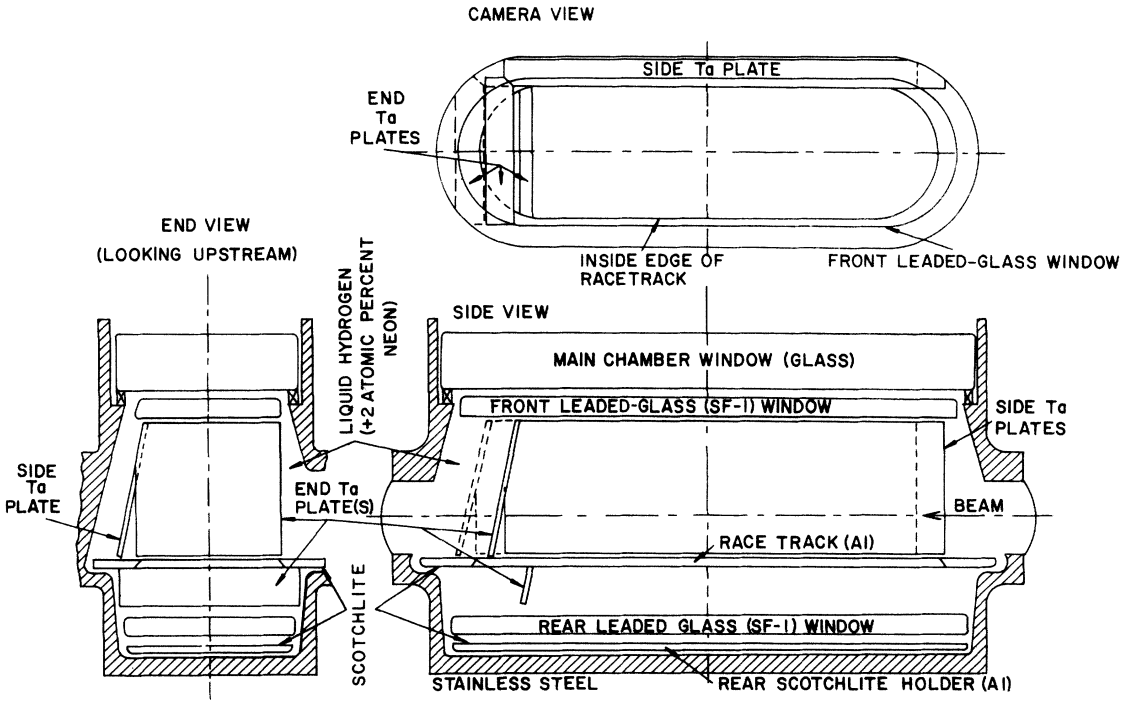

FIG. 1. Schematic of plate array in the BNL 31-in. bubble chamber; three views: camera view, side view, and end view. The main bubble-chamber window, the leaded-glass windows, the tantalum plates, the liquid hydrogen-neon, and the "Scotchlite" retrodirectors are indicated. The tantalum plate array for run 1 was at the position shown dashed; for runs 2 and 3 it was moved to the (solid) position shown with the additional piece added near the rear glass plate.

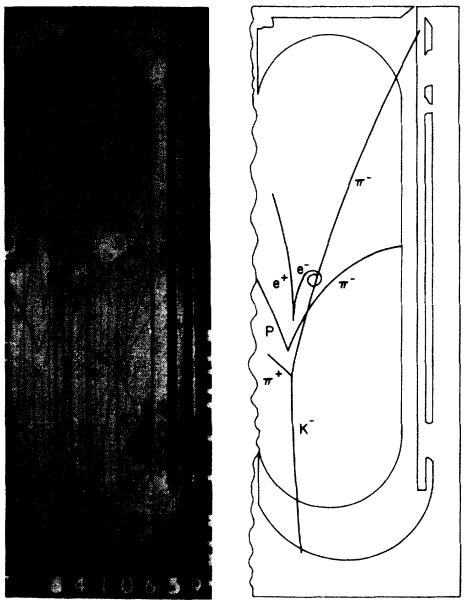

FIG. 2. View 1 of photograph 8 410 659 (roll 841) and line drawing showing an event $K^-p \to \Lambda\eta'$, $\eta' \to \pi^+\pi^-\gamma$, $\gamma \to e^+e^-$ in the chamber liquid.

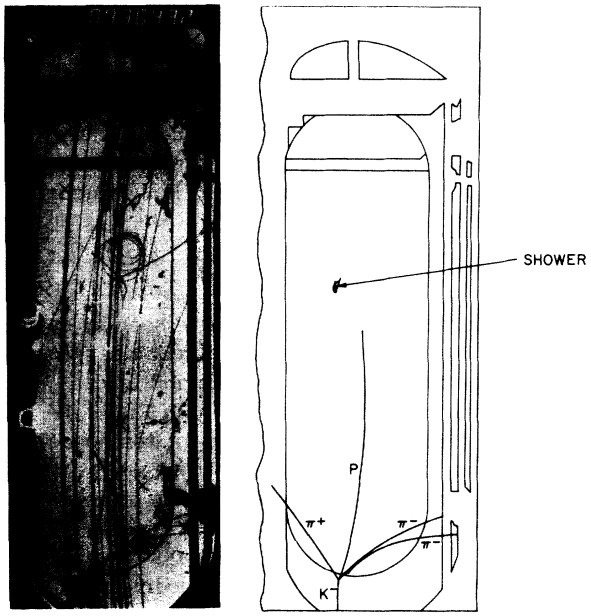

FIG. 3. View 1 of photograph 0 930 431 (roll 93) (number showing here is for the next frame) and line drawing showing an event $K^-p \to \Lambda\eta'$, $\eta' \to \pi^+\pi^-\gamma$, $\gamma \to$ shower in the rear leaded-glass window.

$$K^-p \to \Lambda\pi^+\pi^-\gamma \quad (1)$$
$$\to \Lambda\pi^+\pi^-\pi^0 \quad (2)$$
$$\to \Lambda\pi^+\pi^- \text{ MM} \quad (3)$$
$$\to \Xi^-K^+\gamma \quad (4)$$
$$\to \Xi^-K^+\pi^0. \quad (5)$$

Events fitting the more highly constrained or more copious reactions

$$K^-p \to \Lambda\pi^+\pi^- \quad (6)$$
$$\to \Sigma^0\pi^+\pi^- \quad (7)$$
$$\to \Xi^-K^+ \quad (8)$$
$$\to \Xi^-K^0\pi^+ \quad (9)$$

are eliminated (vetoed). In the case of reaction (7), the elimination is done by excluding events fitting reaction (1) which have a Λ-γ mass $M(\Lambda\gamma) < 1.22$ GeV. In addition, for reactions (1) and (2) only those events having a four-momentum transfer to the Λ, $-t_{p,\Lambda} < 0.7$ GeV^2, are used. The choice between reactions (1) and (2) is generally made by a cut on MM^2 at 0.019 GeV^2.

The selection of γ events began with scanning and measuring of all events without regard to showers, as described in earlier papers.[1,2] Next, various reaction classes, such as (1)–(5) above, were selected to be examined for showers. The scanning and preliminary rough digitizing for the first stage was done on image plane digitizing (IPD) equipment at BNL and at the University of Michigan. Precision measurements of all events were obtained from the BNL Hough-Powell digitizer (HPD). The second-stage shower scanning and measuring (IPD) was done solely at the University of Michigan. The shower positions (two view measurements) were digitized; the direction of the photon is the unit space vector from the event vertex in the chamber to these shower positions. For about 85% of the sample (0.9 million pictures) all events fitting reactions (1)–(5) were processed. On a second pass, including the scanning and measuring of the remaining 15% (0.2 million pictures), only events with a mass recoiling against the Λ from 0.9–1.0 GeV were considered for reactions (1), (2), and (3). However, all events corresponding to reactions (4) and (5) were processed.

Those events corresponding to the shower measurements were extracted from the HPD data summaries of the first-stage analysis and merged with the vertex positions of the showers to form the shower data summary. Analysis of this merged data sample and some data from the original HPD data summary are reported here.

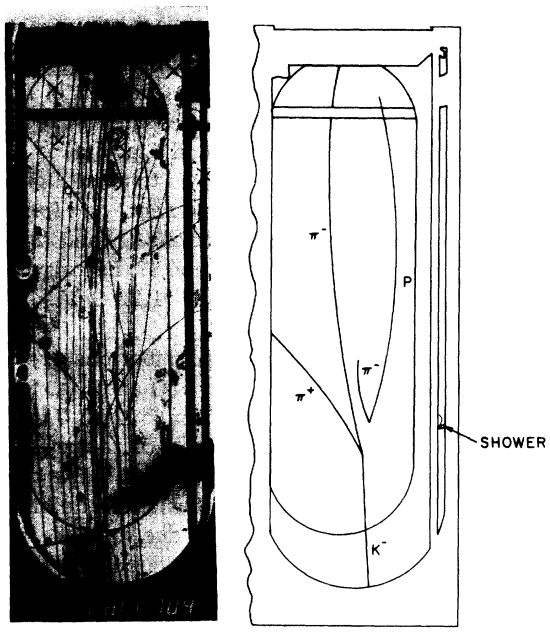

FIG. 4. View 1 of photograph 1 811 704 (roll 181) and line drawing showing an event $K^-p \to \Lambda\eta'$, $\eta' \to \pi^+\pi^-\gamma$, $\gamma \to$ shower in the side tantalum plate.

IV. ANALYSIS OF THE SINGLE-γ SIGNAL

Only the direction of the γ from the shower measurement is used in this analysis. Single-photon decays produce a γ ray close in the direction of the momentum of the neutral particle while π^0's, which decay to two γ's, produce showers at various angles relative to the π^0 momentum. In the rest frame of the π^0, an isotropic decay angular distribution is expected. Anisotropic detection efficiency and background from unassociated showers are expected to contaminate the raw data.

For each shower we calculate

$$\cos\theta^* = (\cos\gamma - \beta)/(1 - \beta\cos\gamma), \quad (10)$$

where θ^* is the angle of the photon in the parent's rest frame (the parent is usually assumed to be a π^0), γ is the laboratory space angle between the direction of the parent and the shower, and β is the velocity (v/c) of the parent in the laboratory system.

The distributions of $\cos\theta^*$ for all γ's are shown in Fig. 5; about two showers per event were found on the average. For events having a missing mass squared (MM^2) less than one pion mass squared (about 0.019 GeV^2) the fits corresponding to reaction (1) were used and are displayed in Fig. 5(a); for larger MM^2, the fits corresponding to reaction (2) were used and are displayed in Fig. 5(b). A peak of 135 events near $\cos\theta^* = 1$ in Fig. 5(a) con-

stitutes evidence for single-γ modes of reaction (1). There is no corresponding peak in Fig. 5(b). The MM^2 cut for Fig. 5(b) excludes the tail of the MM^2 distribution of true single-γ events. The width of the peak near $\cos\theta^* = 1$ in Fig. 5(a) is appropriate for γ directions known to about 0.5–1 degree from the shower measurement, and for fitted neutral directions in reactions (1) and (2) known to 1 or 2 degrees. Reaction (7) has already been eliminated by the cut $M(\Lambda\gamma) > 1.22$ GeV for reaction (1).

Gross features of the $\cos\theta^*$ distributions are caused by backgrounds. In Fig. 5(a) and Fig. 5(b) a relatively flat distribution in $\cos\theta^*$ from 0 to 0.9 or 1.0, respectively, corresponds to the isotropic decay of a π^0 where the forward γ has been detected. The rise of the distribution in the backward region toward $\cos\theta^* = -1$ is due to background γ's from other sources. The $\cos\theta^*$ values from a sample of false associations are shown for all events corresponding to reactions (1) and (2) in Fig. 5(c). The false associations are obtained by using the direction of a shower in some event with another event; in practice, the direction of the γ from one accepted event was used with the next accepted event. A distribution that falls more sharply towards $\cos\theta^* = 1$ without becoming as flat as it did in Figs. 5(a) and 5(b) is observed. The backward peaks in Figs. 5(a) and 5(b) are compatible with γ's from false associations.

The $\cos\theta^*$ distributions for the events of reactions (1) and (2) with one shower or the "best" shower if more than one, i.e., that shower giving the largest $\cos\theta^*$, have features similar to those shown in Fig. 5. They are less peaked at $\cos\theta^* = -1$, however, and the corresponding background distribution for false associations falls faster in the forward direction. We estimate that about 80% of the events in the isotropic region for $\cos\theta^* > 0$ represent π^0 decays with one seen γ and that the balance is due to background.

Kinematic fits which include the γ-shower measurements for all events near $\cos\theta^* = 1$ do not resolve reactions (1) and (2). Instead we use cuts on $\cos\theta^*$ to isolate examples of reaction (1).

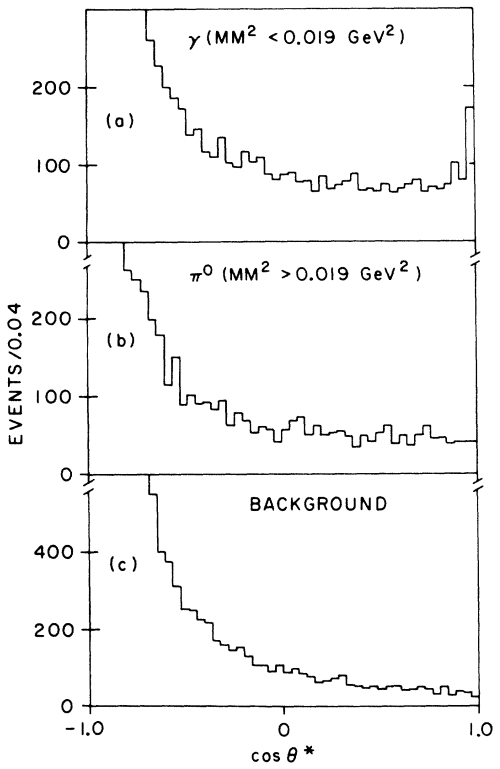

FIG. 5. Distributions in $\cos\theta^*_\gamma$ (see text) for all events excluding Σ^0, i.e., $M(\Lambda\gamma) > 1.22$ GeV fitting (a) $K^-p \to \Lambda\pi^+\pi^-\gamma$ ($MM^2 < 0.019$ GeV^2), (b) $K^-p \to \Lambda\pi^+\pi^-\pi^0$ ($MM^2 > 0.0019$ GeV^2), and (c) falsely associated γ's for reactions of (a) and (b) (see text).

V. ISOLATION OF THE DECAY $\eta' \to \rho^0\gamma$

Figure 6 shows the $\cos\theta^*$ distributions (for $\cos\theta^* > 0.2$) for the "best" shower for the events of reaction (1), excluding events having $M(\Lambda\gamma) < 1.22$ GeV. Figure 6(a) shows the distribution in $\cos\theta^*$ for all events, whereas Fig. 6(b) is the corresponding one for those events containing a ρ meson, that is, with the $\pi^+\pi^-$ mass satisfying $0.62 < M(\pi^+\pi^-) < 0.88$ GeV. The shaded region is the $\cos\theta^*$ distribution for the "best" false-association choice. The slanted dashed lines represent the isotropic decay distribution of π^0's and of the false associations. For $\cos\theta^* > 0.8$, we find 135 events and 118 events above those dashed lines in Fig. 6(a) and Fig. 6(b), respectively.

Next we make cuts on $\cos\theta^*$ and plot the mass distribution $M(\pi^+\pi^-\gamma)$ of the events in Fig. 7. The events with $\cos\theta^* > 0.88$ are shown as the outer solid lines and the events with a more restrictive cut, $\cos\theta^* > 0.94$, are shown shaded. Figure 7(a) corresponds to all events of reaction (1), $MM^2 < 0.019$ GeV^2 with no $M(\pi^+\pi^-)$ cut [as in Fig. 6(a)]; Fig. 7(b) corresponds to the ρ cut events of Fig. 6(b). Figure 7(c) shows the corresponding plot for events of reaction (2), $MM^2 > 0.019$ GeV^2. We see a clean η' signal with little background in Figs. 7(a) and 7(b); there is no η' signal in Fig. 7(c). Thus, the data of Figs. 7(a) and 7(b) between the limits labeled "cut," $M(\pi^+\pi^-\gamma) = 0.958 \pm 0.025$ GeV, represent a nearly pure sample ($\geq 90\%$ pure) of $\eta' \to \pi^+\pi^-\gamma$ in which all the decay products have been detected.

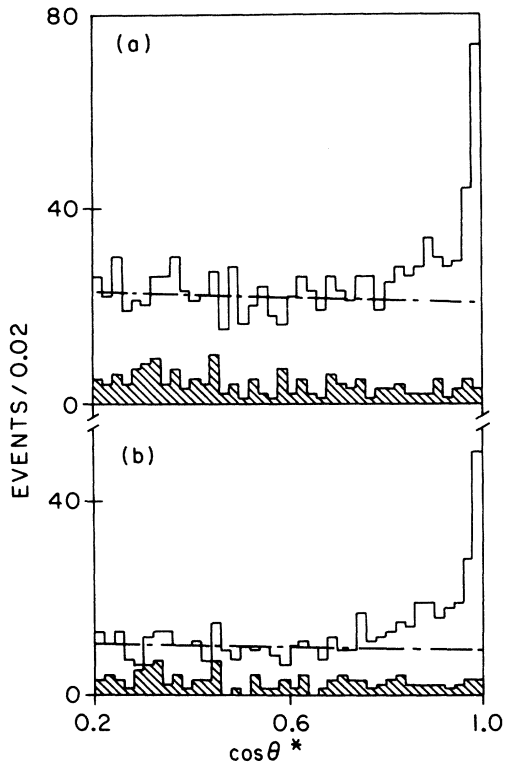

FIG. 6. Distributions of $\cos\theta_\gamma^*$ for the "*only*" or the "best" γ for $\Lambda\pi^+\pi^-\gamma$ events [$MM^2 < 0.019$ GeV^2 and $M(\Lambda\gamma) > 1.22$ GeV]. (a) All events (open) and "false associations" (shaded); (b) for ρ cut, $0.62 < M(\pi^+\pi^-) < 0.88$ GeV (open) and "false associations" (shaded). The peaks in the distributions near $\cos\theta_\gamma^* = 1$ are evidence for real $\Lambda\pi^+\pi^-\gamma$ events. The dot-dash lines represent the $\cos\theta_\gamma^*$ distribution of the background from $\pi^0 \to 2\gamma$ and "false associations."

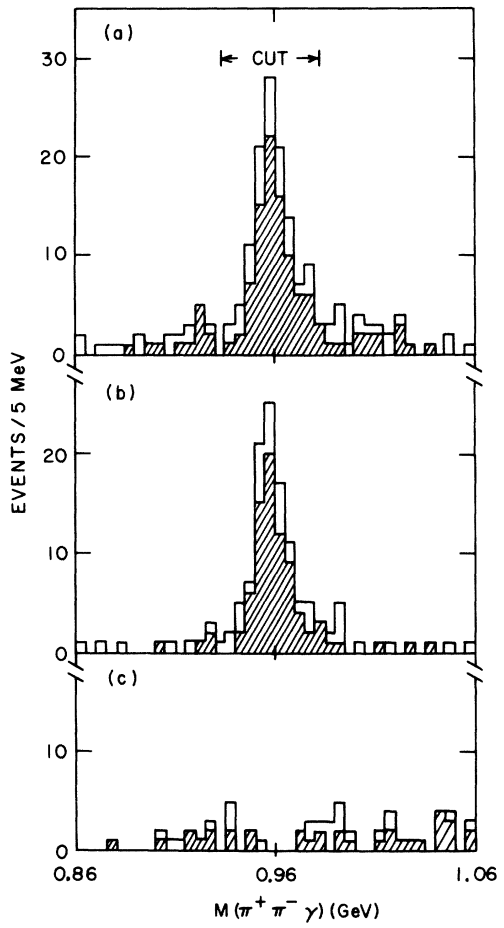

FIG. 7. The $M(\pi^+\pi^-\gamma)$ distributions of the events of Fig. 6 with $\cos\theta_\gamma^* > 0.88$ (outer solid line) and a more restrictive cut $\cos\theta_\gamma^* > 0.94$ (shaded). (a) corresponds to Fig. 6(a), all $M(\pi^+\pi^-)$ masses; (b) corresponds to Fig. 6(b), the ρ cut $0.62 < M(\pi^+\pi^-) < 0.88$ GeV; (c) corresponds to $\Lambda\pi^+\pi^-\pi^0$ ($MM^2 > 0.019$ GeV^2). The clean η' peaks in (a) and (b) account for all of the $\Lambda\pi^+\pi^-\gamma$ event peaks near $\cos\theta_\gamma^* = 1$ in Figs. 6(a) and 6(b).

We show the Dalitz-plot projections $M(\pi^+\pi^-)$ and $\cos\theta_{\pi^+\gamma}$ (see Ref. 1 for the normal analyses) for the events of Figs. 7(a) and 7(b) within the indicated "cut" in Fig. 8(a) and Fig. 8(b), respectively. Figures 8(c) and 8(d) show the corresponding distributions for sidebands on either side of the "cut" region. The solid curves in Figs. 8(a) and 8(b) represent the expectations from the $J^P = 0^-$ matrix element including the ρ-meson final-state interaction. We see that this matrix element describes the data. Most previous analyses of the $\eta' \to \pi^+\pi^-\gamma$ decay had to be made after subtraction of a large $\pi^+\pi^-\pi^0$ background.[1]

In addition, we see that there is no asymmetry in the $\cos\theta_{\pi^+\gamma}$ distribution in Fig. 8(b). In fact, the distribution is quite consistent with the $\sin^2\theta$ curve shown. The asymmetry $\alpha = (N_+ - N_-)/(N_+ + N_-)$, where N_+ = number of events with $\cos\theta_{\pi^+\gamma} > 0$ and N_- = number of events with $\cos\theta_{\pi^+\gamma} < 0$, is $\alpha = 0 \pm 0.1$. This is to be compared with the background-subtracted value $\alpha = +0.07 \pm 0.08$ found by Rittenberg and Kalbfleisch.[3] The pure sample here gives greater confidence that there is no asymmetry present to the 10% level. We note that this result is as significant a result against C-invariance violation as that obtained from $\eta(549) \to \pi^+\pi^-\gamma$ decays. According to Barrett and Truong,[4] a C-violating electromagnetic amplitude yielding an $\alpha = 0.1$ asymmetry in $\eta' \to \rho^0\gamma$ decay will result in a much smaller asymmetry in $\eta(549) \to \pi^+\pi^-\gamma$ decay, namely, $\alpha_\eta = 0.004$. This is to be compared with the result $\alpha(\eta(549)) = 0.005 \pm 0.006$ from 36 155 events of Thaler *et al.*,[5] and with the result $\alpha(\eta(549)) = 0.012 \pm 0.006$ from the 34 680 events of Jane *et al.*[6]

VI. SEARCH FOR THE DECAY $\eta \to \omega\gamma$

A "0C" calculation can be made for a process such as

$$K^- p \to \Lambda \pi^+ \pi^- \pi^0 \gamma \qquad (11)$$

when the direction of the direct γ is observed. We iterate a series of calculations on each γ of each event. Some subset of the events and γ showers yields self-consistent solutions and these solutions are studied. The iterative series of calculations is as follows: (i) Assume a mass for $M(\pi^+\pi^-\pi^0)$ in reaction (11), where $M(\pi^+\pi^-) < M(\pi^+\pi^-\pi^0) < M(\pi^+\pi^-\text{MM})$, where MM is the missing mass in reaction (3). Then (ii) calculate a $\cos\theta$ as in Eq. (10), except that the recoil mass off the Λ, $M(\pi^+\pi^-\text{MM})$, is used in place of the π^0-mass hypothesis of Eq. (10). Using $\cos\theta^*$ for the $M(\pi^+\pi^-\pi^0)$ mass assumed, (iii) a Lorentz transformation to the laboratory system is made, and (iv) the four-vector of the missing π^0 is computed. A self-consistent solution exists if the square of this four-vector is closely equal to the π^0 mass squared. If this does not hold, the value of $M(\pi^+\pi^-\pi^0)$ is increased and the iterative procedure continues. If there are no self-consistent solutions, that γ shower and/or event is rejected, and the search continues until the complete sample of events has been examined.

In order to search for $\eta' \to \omega\gamma$, this iterative procedure has been applied to a subset of the events fitting reactions (2) and (3) which would contain events of reaction (11). Since the iterative procedure has no constraints (i.e., is "0C") we restrict the sample to enhance possible η' and ω signals and reduce backgrounds. A more restrictive $-t_{p,\Lambda}$ cut is taken, $-t < 0.35$ GeV^2, which accepts 0.8 of the η' mesons produced with $-t < 0.7$ GeV^2 (cf. Fig. 38 of Ref. 1). An $M(\pi^+\pi^-)$ cut is taken which takes advantage of the decay matrix element of the ω and eliminates feedthrough of other decay modes of the η'; we chose $0.41 < M(\pi^+\pi^-) < 0.61$ GeV. The lower cut eliminates $\eta' \to \pi^+\pi^-\eta$ events and the upper cut eliminates most $\eta' \to \rho^0\gamma$ events and retains a fraction 0.67 of all ω mesons. This "cut" on the $M(\pi^+\pi^-)$ of ω mesons is shown in Fig. 9, where the $M(\pi^+\pi^-)$ mass distribution of all events fitting reactions (1) or (2) is displayed for events having $M(\pi^+\pi^-\pi^0) = 783 \pm 30$ MeV. The effect of these two cuts on the search for $\eta' \to \omega\gamma$ is taken into account later.

Having made these cuts we show in Fig. 10 the distribution of $M(\pi^+\pi^-\pi^0)$ from the iterative solution for reaction (11) for all events having $M(\pi^+\pi^-\text{MM})$ in the η' band, 958 ± 25 MeV, and satisfying the two cuts discussed above. We see no excess at 783 MeV and set an upper limit of 10 events at 90% confidence level (C.L.).

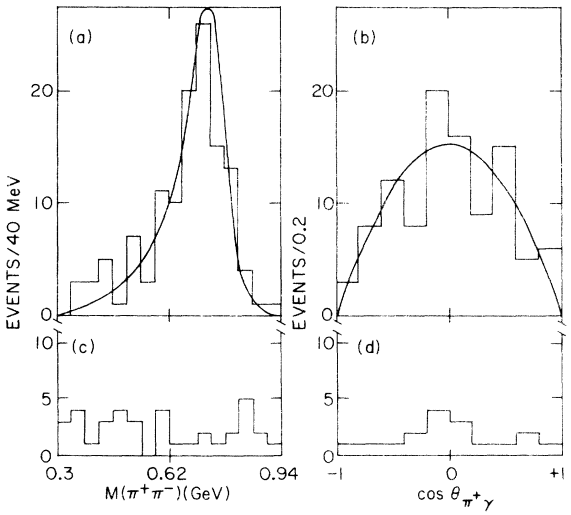

FIG. 8. The $M(\pi^+\pi^-)$ and $\cos\theta_{\pi^+\gamma}$ Dalitz-plot projections of the η' data for "cut," $M(\pi^+\pi^-\gamma) = 958 \pm 25$ MeV shown in Figs. 7(a) and 7(b). (a) $M(\pi^+\pi^-)$ for data of Fig. 7(a) with $J^P = 0^-$ curve for the matrix element including ρ-meson final-state interaction. (b) $\cos\theta_{\pi^+\gamma}$ for data of Fig. 7(b), with ρ cut; curve is $\sin^2\theta$ expected for $J^P = 0^-$. (c) $M(\pi^+\pi^-)$ for events of Fig. 7(a) in bands adjacent to "cut" band on either side. (d) $\cos\theta_{\pi^+\gamma}$ for events in Fig. 7(b) in bands adjacent to "cut" band on either side.

Correcting for the effects of the cuts and normalizing to the kinematically similar 135 $\eta' \to \rho\gamma$ events discussed above we obtain

$$R_1 = \frac{\eta' \to \omega\gamma}{\eta' \to \rho^0\gamma} = \frac{\leq 10/(0.67 \times 0.8)}{135} \leq 0.15 \ (90\%\ \text{C.L.}).$$

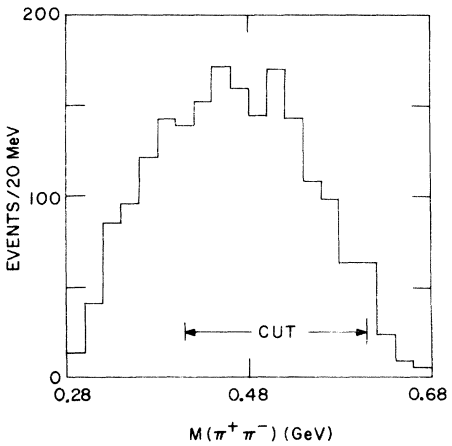

FIG. 9. The $M(\pi^+\pi^-)$ distribution for $\omega(783)$ events from the reaction $K^- p \to \Lambda\pi^+\pi^-\pi^0$ with $M(\pi^+\pi^-\pi^0) = 783 \pm 30$ MeV. The "cut" is used to enhance the ω signal in $\eta' \to \omega\gamma$ search and exclude $\eta' \to \eta\pi^+\pi^-$ and $\eta' \to \rho\gamma$ decays.

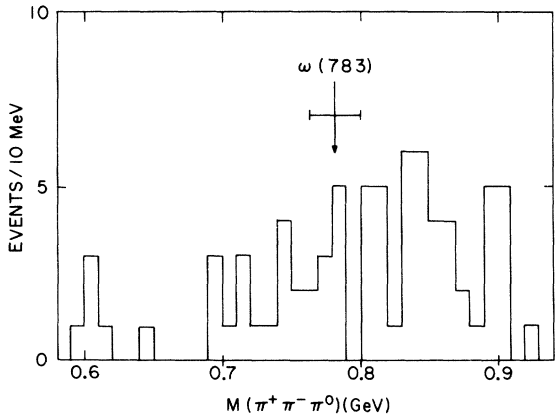

FIG. 10. The $M(\pi^+\pi^-\pi^0)$ spectrum (see text) for search for $\eta' \to \omega\gamma$. No ω enhancement is seen.

Using our result for the $\eta' \to \rho^0\gamma$ branching ratio of 0.30 ± 0.03 (see Table III of Ref. 1), we obtain

$$R_2 = \frac{\eta' \to \omega\gamma}{\eta' \to \text{all}} \leq 0.05 \text{ (90\% C.L.)}$$

from a direct search. This is to be compared to Rittenberg's value[7,8] for $R_2(\eta' \to \omega\pi^0(\text{or}\gamma)) < 0.08$ (67% C.L.) using indirect "kinematic" cuts. The ratio $R_1 < 0.15$ (90% C.L.) is to be compared with an SU_3 prediction of $R_1 \sim 0.1$ given by Dalitz and Sutherland[9] for a $J^P = 0^-$ η' meson mixing with the $\eta(549)$.

VII. SEARCH FOR $\omega(783)$ AND $\phi(1019) \to \pi^+\pi^-\gamma$

The peak in $\cos\theta$ near 1 in Fig. 5(a) was seen to be accounted for by $\eta' \to \rho^0\gamma$. In Fig. 11(a) and Fig. 11(b) are shown the $\cos\theta^*$ distributions for the best shower for recoil masses $M(\pi^+\pi^-\gamma(\text{or}\pi^0))$ in reactions (1) or (2) about the ω, 0.763 GeV $< M(\pi^+\pi^-\gamma(\text{or}\ \pi^0)) < 0.803$ GeV, and ϕ, 1.009 $< M(\pi^+\pi^-\gamma(\text{or}\ \pi^0)) < 1.029$ GeV, respectively. The reaction (1) events with $MM^2 < 0.019$ GeV^2 are shown shaded and the reaction (2) events with $MM^2 > 0.019$ GeV^2 as the open area. No excess of events near $\cos\theta = 1$ is observed. The shaded distributions give an upper limit of ≤ 8 events and ≤ 6 events for the ω and ϕ regions, respectively. The 100 events in Fig. 11(a) represent $\omega \to \pi^+\pi^-\pi^0$, where 1γ from the decay $\pi^0 \to 2\gamma$ is detected; this γ has similar kinematic properties to γ's from any possible $\omega \to \pi^+\pi^-\gamma$ decays. We, therefore, use these events for the denominator in computing $R = (\omega \to \pi^+\pi^-\gamma)/(\omega \to \text{all})$. We must correct the $\omega \to$ all denominator for $\omega \to \pi^0\gamma$ (factor of 1.1), background under the ω, background in Fig. 11(a), and the $\cos\theta > 0.5$ cut (factor of 2). The $\omega \to \pi^+\pi^-\pi^0$ signal for all events of reaction (2) with or without a γ shower detected is shown in Fig. 12(a), where

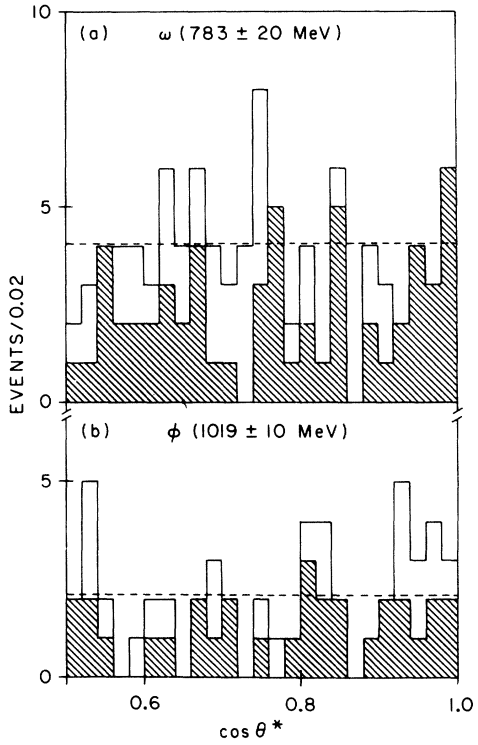

FIG. 11. The $\cos\theta^*_\gamma$ distributions for $\Lambda\pi^+\pi^-(\gamma/\pi^0)$ events in the ω and ϕ regions. (a) ω region $M(\pi^+\pi^-\gamma(\text{or}\ \pi^0)) = 783 \pm 20$ MeV. (b) ϕ region $M(\pi^+\pi^-\gamma(\text{or}\ \pi^0)) = 1019 \pm 20$ MeV. The open regions are for π^0; the shaded regions are for γ events. No enhancements are observed near $\cos\theta^* = 1$; upper limits for the decays $\omega, \phi \to \pi^+\pi^-\gamma$ are obtained (see text).

about 1330 events are observed above the indicated dashed background level. The background level in the 783 ± 20 MeV region is about 20%. The background of unassociated γ showers in Fig. 11(a) was discussed in general above and found to about 20%. Thus we find

$$R = \frac{\omega \to \pi^+\pi^-\gamma}{\omega \to \text{all}}$$

$$= (\leq 8)/(0.8 \times 0.8 \times 1.1 \times 2 \times 100)$$

$$= \frac{\leq 8}{140} \leq 0.06 \text{ (90\% C.L.)}.$$

Using $\Gamma_\omega = 10.0 \pm 0.4$ MeV,[8] we find

$$\Gamma(\omega \to \pi^+\pi^-\gamma) < 0.6 \text{ MeV (90\% C.L.)}.$$

This direct-search result is to be compared with $R < 0.05$ (67% C.L.) from the indirect search of Flatté *et al.*[10]

The corresponding result for the $\phi(1019)$ is obtained from the ratio of ϕ and ω events in our experiment. Figure 12(b) shows the mass distribution for $\phi \to K^+K^-$ from the reaction

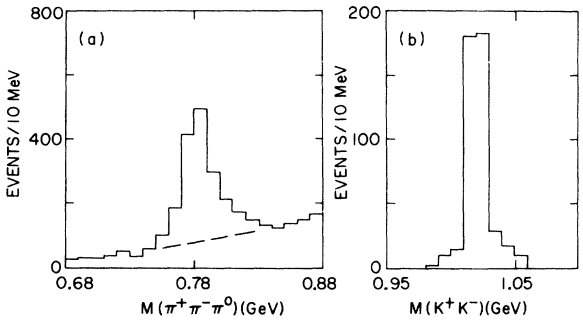

FIG. 12. The (a) $M(\pi^+\pi^-\pi^0)$ and (b) $M(K^+K^-)$ distributions for the reactions $K^-p \to \Lambda\pi^+\pi^-\pi^0$ and ΛK^+K^-. The ϕ/ω ratio is needed for the branching ratio $\phi \to \pi^+\pi^-\gamma$ (see text).

$$K^-p \to \Lambda K^+K^- . \tag{12}$$

The number of $\phi \to K^+K^-$ events is estimated to be 470. This gives, correcting for the branching ratio of $\phi \to K^+K^-$,[8] the ϕ/ω ratio

$$R(\phi/\omega) = \frac{470/0.47}{1330} = 0.75 \pm 0.06 .$$

Thus, we find

$$R = \frac{\phi \to \pi^+\pi^-\gamma}{\phi \to \text{all}}$$

$$= \frac{\leq 6}{0.75 \times 140} \leq 0.06 \text{ (90\% C.L.)}.$$

Using $\Gamma_\phi = 4.2 \pm 0.2$ MeV,[8] we find

$$\Gamma(\phi \to \pi^+\pi^-\gamma) < 0.2 \text{ MeV (90\% C.L.)}.$$

This is to be compared with the result of Cosme *et al.*[11] of 0.7% (0.03 MeV) (90% C.L.) from the storage-ring study of $e^+e^- \to \phi \to \pi^+\pi^-\pi^0$ (or γ).

VIII. SEARCH FOR THE DECAY $\Xi^{*-}(1535) \to \Xi^-\gamma$

We have previously discussed the data on $\Xi^{*0}(1531)$ in our data.[2] We show the much smaller signal for $\Xi^{*-}(1535)$ in reaction (5) for all data in Fig. 13. We estimate that there are 60 ± 10 examples of $\Xi^{*-}(1535) \to \Xi^-\pi^0$, which represents one third of the Ξ^{*-} signal. The other two thirds corresponds to decay to $\Xi^0\pi^-$, generally inaccessible to the low momentum transfer to the Λ scanning technique[1] employed in this experiment.

We show in Fig. 14(a) the distribution of $\cos\theta^*$ via Eq. (10) for those events of reactions (4) and (5) having $M(\Xi^-\pi^0$ or $\gamma) = 1535 \pm 80$ MeV. The shaded events represent those of reaction (4) with $MM^2 < 0.019$ and in the Ξ^{*-} mass band 1535 ± 10 MeV; no peak is observed near $\cos\theta = 1$. We attribute 0 events with an upper limit of 2.3 (90% C.L.)

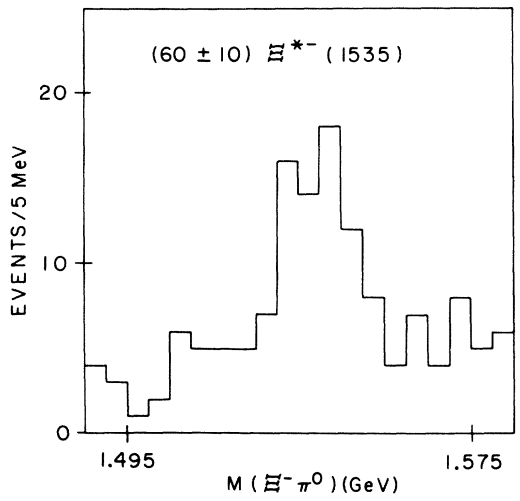

FIG. 13. The $M(\Xi^-\pi^0)$ spectrum of all the events fitting $K^-p \to \Xi^-K^+\pi^0$. We estimate 60 ± 10 $\Xi^{*-}(1535) \to \Xi^-\pi^0$ events are present in the total sample.

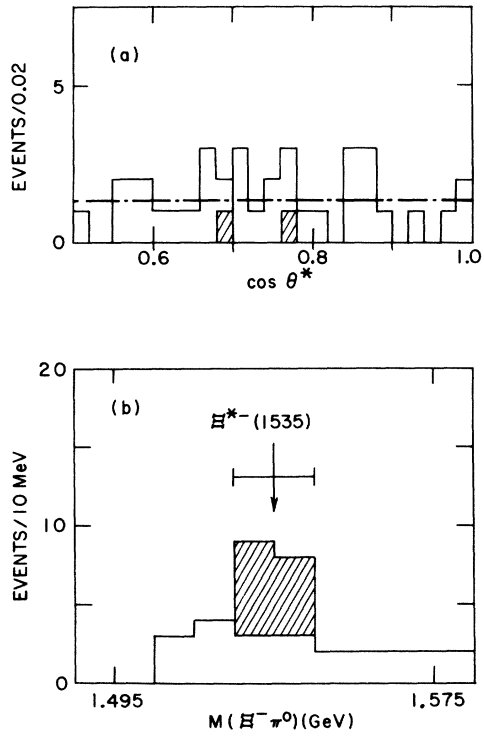

FIG. 14. (a) The $\cos\theta_\gamma^*$ distribution (open) for all $K^-p \to \Xi^-K^+\pi^0$ events with a γ shower observed, for $M(\Xi^-\pi^0) = 1535 \pm 80$ MeV, and for $K^-p \to \Xi^-K^+\gamma$ (shaded) for $M(\Xi^-\pi^0) = M(\Xi^{*-}(1535)) = 1535 \pm 10$ MeV. (b) The $M(\Xi^-\pi^0)$ distribution for the events of (a). A minimum of 11 events, shown shaded, is estimated for the denominator of the $\Xi^-\gamma/\Xi^-\pi^0$ branching ratio.

to the decay $\Xi^{*-}(1535)\to\Xi^-\gamma$. In Fig. 14(b) we show the $M(\Xi^-\pi^0)$ mass distribution of the events of Fig. 14(a). We see a signal of ≥ 11 $\Xi^{*-}(1535)$ events, shown shaded. Correcting for the $\cos\theta > 0.5$ cut (factor of 2) and the unobserved decay mode $\Xi^0\pi^-$ (factor of 3) we find

$$R = \frac{\Xi^{*-}(1535)\to\Xi^-\gamma}{\Xi^{*-}(1535)\to \text{all}} = \frac{0(<2.3(90\%\ \text{C.L.}))}{2\times 3\times(\geq 11)} < 0.04\ (90\%\ \text{C.L.}).$$

Using $\Gamma_{\Xi^{*-}} = 10.6\pm 2.6$ MeV (Ref. 8) (note that[8] $\Gamma_{\Xi^{*0}} = 9.1\pm 0.5$ MeV, we find

$$\Gamma(\Xi^{*-}\to\Xi^-\gamma) < 0.4\ \text{MeV}\ (90\%\ \text{C.L.}).$$

This decay mode is expected to be nonexistent if the photon is a U-spin singlet as normally envisaged, since a decouplet has no SU_3-invariant coupling to an octet plut singlet. This upper limit of 4% (0.4 MeV) can be compared to the observed rate of 0.7% (0.8 MeV) for $\Delta^+(1238)\to p\gamma$.[8]

IX. CONCLUSIONS

We find a relatively pure sample of 135 examples of $\eta'\to\pi^+\pi^-\gamma$ decay with the photon detected. The Dalitz-plot projections show clearly the ρ meson and the $\sin^2\theta_{\pi^+\gamma}$ distributions expected for $J^P = 0^-$ (or 2^-). The angular distribution shows no asymmetry; C-invariance violation is parameterized by the asymmetry $\alpha = 0\pm 0.1$. We have searched for the SU_3-allowed decay mode $\eta'\to\omega\gamma$ but obtain only an upper limit, ≤ 0.05 (90% C.L.). We have also searched for the decay modes $\omega\to\pi^+\pi^-\gamma$, $\phi\to\pi^+\pi^-\gamma$, and $\Xi^{*-}(1535)\to\Xi^-\gamma$ with null results, yielding upper limits for the partial widths of less than a fraction of an MeV.

ACKNOWLEDGMENTS

This experiment depended upon the help of many people. First, many thanks to John Koehler for his dedication to providing and maintaining the tantalum and leaded-glass plates so essential to detecting the photons. Thanks also to Dr. A. Prodell, F. Pechar, and the crew of the 31-in. bubble chamber for their successful operation of the chamber with these plates installed and filled with hydrogen-neon mixtures and under multipulsing conditions. Many thanks also to the many scanning and measuring personnel of both Brookhaven National Laboratory and the University of Michigan, and especially the latter for their additional special shower scanning.

In addition, we acknowledge the help of several physicists associated with various aspects of this experiment over the years; Professor S. R. Borenstein, Dr. J. S. Danburg, Dr. R. K. Kiang, Dr. J. Lys, and Dr. V. VanderBurg. We also gratefully acknowledge the support and encouragement of Professor B. Roe, Dr. N. P. Samios, and Dr. R. P. Shutt.

---

†Work supported by the U. S. Atomic Energy Commission.

[1]J. S. Danburg *et al.*, Phys. Rev. D 8, 3744 (1973).
[2]S. R. Borenstein *et al.*, Phys. Rev. D 5, 1559 (1972).
[3]A. Rittenberg and G. R. Kalbfleisch, Phys. Rev. Lett. 15, 556 (1965).
[4]B. Barrett and T. N. Truong, Phys. Rev. 147, 1161 (1966).
[5]J. J. Thaler *et al.*, Phys. Rev. Lett. 29, 313 (1972).
[6]M. R. Jane *et al.*, Phys. Lett. 48B, 265 (1974).
[7]A. Rittenberg, Ph.D. thesis, University of California, Berkeley, 1969, UCRL Report No. UCRL-18863, 1969 (unpublished).
[8]Particle Data Group, Rev. Mod. Phys. 45, S1 (1973); Phys. Lett. 50B, 1 (1974).
[9]R. H. Dalitz and D. G. Sutherland, Nuovo Cimento 37, 1777 (1965).
[10]S. Flatté *et al.*, Phys. Rev. 145, 1050 (1966).
[11]G. Cosme *et al.*, Phys. Lett. 48B, 155 (1974).

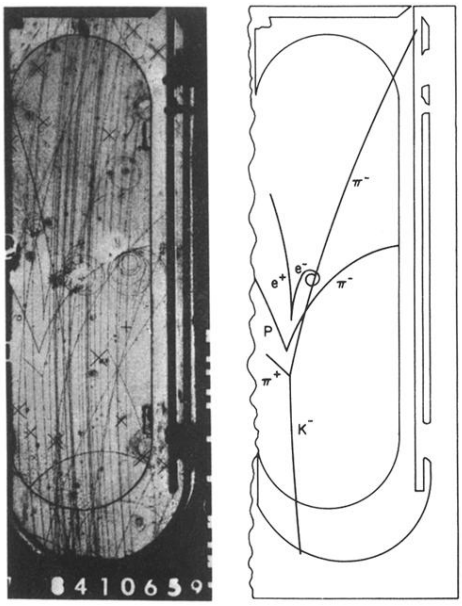

FIG. 2. View 1 of photograph 8 410 659 (roll 841) and line drawing showing an event $K^-p \rightarrow \Lambda\eta'$, $\eta' \rightarrow \pi^+\pi^-\gamma$, $\gamma \rightarrow e^+e^-$ in the chamber liquid.

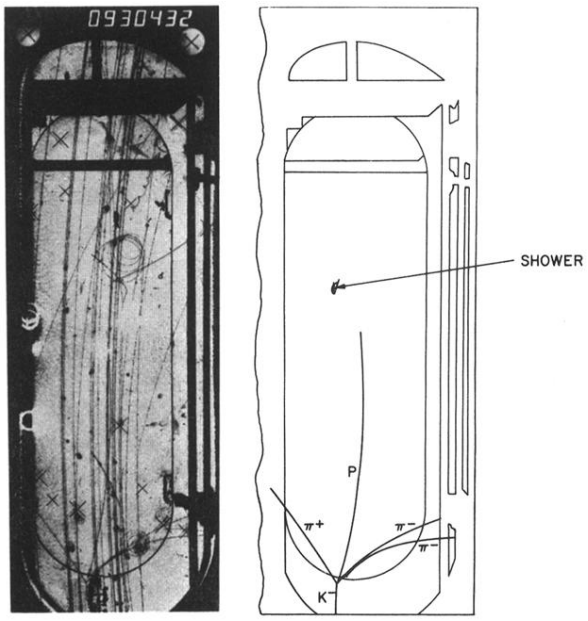

FIG. 3. View 1 of photograph 0 930 431 (roll 93) (number showing here is for the next frame) and line drawing showing an event $K^- p \rightarrow \Lambda \eta'$, $\eta' \rightarrow \pi^+ \pi^- \gamma$, $\gamma \rightarrow$ shower in the rear leaded-glass window.

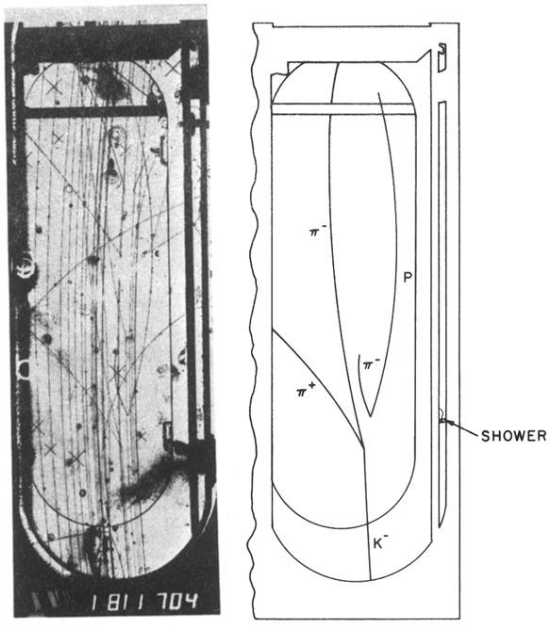

FIG. 4. View 1 of photograph 1 811 704 (roll 181) and line drawing showing an event $K^- p \rightarrow \Lambda\eta'$, $\eta' \rightarrow \pi^+\pi^-\gamma$, $\gamma \rightarrow$ shower in the side tantalum plate.